

# Engineering Entropy for the Inverse Design of Colloidal Crystals from Hard Shapes

Yina Geng,<sup>1,\*</sup> Greg van Anders,<sup>2,1,\*</sup> Paul M. Dodd,<sup>2</sup> Julia Dshemuchadse,<sup>2</sup> and Sharon C. Glotzer<sup>1,2,3,4</sup>

<sup>1</sup>*Department of Physics, University of Michigan, Ann Arbor MI 48109, USA*

<sup>2</sup>*Department of Chemical Engineering, University of Michigan, Ann Arbor MI 48109, USA*

<sup>3</sup>*Department of Materials Science and Engineering, University of Michigan, Ann Arbor MI 48109, USA*

<sup>4</sup>*Biointerfaces Institute, University of Michigan, Ann Arbor MI 48109, USA<sup>†</sup>*

(Dated: March 2, 2022)

Throughout the physical sciences, entropy stands out as a pivotal but enigmatic concept that, in materials design, often takes a backseat to energy. Here, we demonstrate how to precisely engineer entropy to achieve desired colloidal crystals. We demonstrate the inverse design of hard particles that assemble six different target colloidal crystals due solely to entropy maximization. Our approach efficiently samples  $10^8$  particle shapes from 88- and 192-dimensional design spaces to discover thermodynamically optimal shapes. We design particle shapes that self assemble known crystals with optimized thermodynamic stability, as well as new crystal structures with no known atomic or other equivalent.

Our understanding of entropy has undergone three revolutions since its association with lost heat by Clausius in the 1800s.[1] The first is the discovery by Boltzmann [2] and Gibbs [3] of entropy’s central role in statistical mechanics and its colloquial association with disorder. The second is the discovery by Shannon of entropy’s central role in information theory as a quantifier of statistical ignorance.[4] The third is the discovery by Onsager [5] and then by Kirkwood and collaborators [6, 7] of entropy’s seemingly paradoxical implication in ordering hard particles.[8–12] However, after nearly 200 years, entropy has yet to be exploited for design. Engineering entropy is both conceptually and technically difficult because entropy is a globally defined, purely statistical concept. This means there exists no obvious direct link between microscopic, designable details of a system’s components, and the macroscopic order that emerges from entropy maximization. In contrast, pairwise interaction potentials (force fields) between atoms or nanoparticles are now routinely designed for simple self-assembled structures in cases where potential energy, rather than entropy, dominates.[13–19]

Here, we carry out the inverse design of particles that can self-assemble target structures due solely to the emergent effects of entropy arising from their shape, called “shape entropy”.[20] We do this in two steps. The first step begins with randomly generated, arbitrarily shaped convex polyhedra whose shape evolves during a Monte Carlo (MC) simulation by sampling from particle “shape space” via an extended, “alchemical” ensemble.[21] Unlike a traditional molecular MC simulation in which a system of fixed particle shapes samples configurational states in phase space, in an Alchemical Monte Carlo (Alch-MC) simulation particles sample not only positions and orientations but also shapes consistent with the target structure, finding thermodynamically optimal shapes. Alch-MC for polyhedra with  $n$  vertices explore a  $D = 3n - 4$  dimensional parameter space accounting for fixed particle volume and rotational invariance, and produce mathematically irregular but well-defined particle shapes that (i) maximize

the entropy of the target structure and (ii) successfully self-assemble the target structure in a MC simulation starting from a disordered fluid. The second step symmetrizes the designed particles to obtain shapes that still easily assemble the target structure, but because of their symmetry can be made today using existing synthesis methods.[22–25] Depending on the target crystal structure we symmetrized particle shapes either through truncation or through truncation and vertex augmentation. Full simulation details, and mathematical descriptions of all optimal particle shapes are reported in the SI.

We targeted six structures – simple cubic (SC), body-centered cubic (BCC), face-centered cubic (FCC), diamond,  $\beta$ -W, and  $\beta$ -Mn. For  $\beta$ -Mn, FCC and BCC, symmetrized, truncated shapes in step two produced lower free energy crystal structures than sampled unsymmetrized polyhedra found in step one. We give detailed results here for the most complex case,  $\beta$ -Mn; full details for FCC and BCC are given in SI. For  $\beta$ -Mn, the equilibrium distribution of convex polyhedra shapes resulting from our Alch-MC simulations at packing density  $\eta = 0.6$  yields a family of shapes with characteristic dodecahedral facet angles (distribution peaks at  $\approx -0.447$  and  $0.448$ , see Fig. 1d(1), vs. the perfect dodecahedron  $\approx \pm 0.447$ ). Consistent with the particle faceting, potential of mean force and torque (PMFT) calculations [20] for a particle selected from the peak of the shape distribution (Fig. 3a) produced isosurfaces with dodecahedral entropic valence [27]. Symmetry-restricted Alch-MC simulation (see SI for mathematical construction) yielded an optimal truncation with facet area  $0.36$  (Fig. 1d(1)); the peak in facet area differs by less than 3% from the peak observed for the unrestricted shapes ( $0.37$ ). We confirmed using regular MC that shapes generated by Alch-MC simulation spontaneously self assemble the target structure for both the arbitrary convex polyhedron case (depicted in SI Movie 1) and the symmetry-restricted case. To further validate that the particle shape with manifest dodecahedral symmetry is the putative optimal shape, we directly compared the free energy of the target colloidal crystal with the optimal truncated shape using a shape from the peak of the distribution of arbitrary convex shapes (Fig. 1c) and found the symmetric-shape crystal has lower free energy. This result is consistent with our expectation that the free energy landscape of the high-dimensional parameter space of

\* These authors contributed equally to this work.

<sup>†</sup> grva@umich.edu, sglotzer@umich.edu

shapes is rough with nearly degenerate minima. For comparison, we also computed the free energy for a packing-based estimate. There are two Voronoi cells in  $\beta$ -Mn, only one of which can self assemble the structure without enthalpic interactions [11]. We computed the free energy for the Voronoi shape, and found that our approach produced shapes with lower free energy than the particle based on the naive geometric ansatz (Fig. 1c). Fig. 1b shows that Alch-MC converged rapidly to shapes that have lower free energy than the Voronoi ansatz by  $\approx 0.8k_B T$  per particle, and implies the existence of a large space of shapes that are all better than the geometric ansatz. The simulation trajectory shown in Fig. 1b explores  $\gtrsim 10^6$  shapes that have lower free energy in the target structure than the geometric ansatz. Consistent results were found for BCC (Fig. 1d(2)) and FCC (Fig. 1d(3)) target structures (details in SI). The connection between faceting and the emergence of entropic valence with local structural order is robust (BCC–Fig. 2b; FCC–Fig. 2c). In the second step we repeat the procedure using symmetric truncated shapes suggested by the shapes observed in the first step. In all cases we obtained lower free energy shapes than the geometric ansatz ( $\beta$ -Mn  $-0.84 \pm 0.02 k_B T$ ; FCC  $-0.917 \pm 0.002 k_B T$ ; BCC  $-0.337 \pm 0.003 k_B T$ ) (see Fig. 1c).

For  $\beta$ -W, SC and diamond, we found that unsymmetrized polyhedra had lower free energy than symmetrized truncated polyhedra. For these crystals, we implemented step two using symmetrized, truncated, vertex-augmented polyhedra. We give detailed results here for the most complex case,  $\beta$ -W; full details for SC and diamond are given in the SI. For  $\beta$ -W, Alch-MC simulation of unsymmetrized shapes yielded an equilibrium distribution of convex polyhedra with facet angle distribution peaks at  $\pm 0.458$  (Fig. 1d(4)). Like for  $\beta$ -Mn, this falls near the peaks for dodecahedra, but for  $\beta$ -W the facet area distribution is bimodal, indicating, and confirmed by visual inspection, the existence of two large parallel facets. Faceting is again consistent with emergent entropic valence (Fig. 2d) evident in isosurfaces of PMFT measurements [20]. Free energy calculations (Fig. 1c) confirm that a geometric ansatz shape has  $0.815 \pm 0.004 k_B T$  more free energy per particle in the target crystal than a shape at the peak of the distribution of convex shapes. We also confirmed that peak shapes self-assemble the target structure with regular MC (see SI Fig. S2). In contrast to the case 1 structures, Alch-MC of symmetrized shapes restricted to a two-parameter family of truncated dodecahedra yielded shapes with lower free energy in the target  $\beta$ -W structure than the geometric ansatz, but higher free energy than for shapes at the peak of the distribution of convex polyhedra. This finding indicates that the restriction to truncation alone is too severe for  $\beta$ -W. Alch-MC simulation of a refined truncated dodecahedron with vertex-augmented faces (see SI for precise construction) converged to a shape with  $0.999 \pm 0.003 k_B T$  lower free energy per particle than the geometric ansatz. Truncated and augmented free energy minimizing shapes were also

found for SC and diamond (Fig. 1c), which again preserve the connection between faceting and entropic valence (SC–Fig. 2e; diamond–Fig. 2f). Because this facet–valence connection persists, the facet area distributions for SC (Fig. 1d(5)) and diamond structures (Fig. 1d(6)) are unimodal due to the simpler local structural motif in those structures compared to  $\beta$ -W where the facet area distribution is bimodal (Fig. 1d(4)).

Finally, we targeted the self-assembly of a hypothetical structure with no known atomic or other equivalent. The structure is a modified version of the hexagonally-close packed (hcp) structure with distorted lattice spacing, so that particles have eight nearest neighbors, see Fig. 3, whereas hcp has 12. We denote this structure as hP2-X. Alch-MC simulations of convex polyhedra with 116 vertex parameters yielded the faceted shape shown in Fig. 3. We tested that the particle chosen from the peak of the distribution of the cosine of dihedral angles spontaneously self-assembled the target structure from a disordered fluid, with the resulting structure shown in Fig. 3. This demonstrates the inverse design of a colloidal particle shape to entropically stabilize a previously unknown target structure using only digital alchemy [21].

Particle shape has, in principle, an infinite-dimensional parameter space. Here, for tractability, and motivated by shapes that can be realized using nanoparticle synthesis techniques, we searched for optimal particle shapes over 92- and 188-dimensional parameter spaces of convex shapes, using a precisely defined entropic design criterion. Our method yields both optimal particle shapes, but also distributions of candidate shapes that provide insight into the sensitivity of structure to shape features (Fig. 1d). More details of shape sensitivity will be reported elsewhere. Emergent entropic valence that is commensurate with the emergence of faceting in an ensemble of arbitrary convex polyhedra, both of which are, in turn, commensurate with local structural coordination, is a strong indication in favor of the hypothesized connection between faceting, emergent directional entropic forces, and structural order [20, 27]. By consistently establishing the connection between the emergence of faceting and entropic valence, our results suggest future work could assume this connection, and either skip our intermediate step of facet characterization by reading particle faceting directly from PMFT measurements, and/or rather than working agnostically, start the Alch-MC shape evolution working from a Voronoi cell shape.

We thank P. F. Damasceno for discussions. This material is based upon work supported in part by the U.S. Army Research Office under Grant Award No. W911NF-10-1-0518, and by a Simons Investigator award from the Simons Foundation to S. C. G. Simulations were supported through computational resources and services supported by Advanced Research Computing at the University of Michigan, Ann Arbor. J. D. acknowledges support through the Early Postdoc.Mobility Fellowship from the Swiss National Science Foundation, grant number P2EZP2\_152128.

[1] R. Clausius, *Abhandlungen Über Die Mechanische Wärmetheorie* (Friedrich Vieweg und Sohn, Braunschweig, 1864).

[2] L. Boltzmann, *Vorlesungen über Gastheorie* (Johann Ambro-

- sius Barth, Leipzig, 1896).
- [3] J. W. Gibbs, *Elementary Principles in Statistical Mechanics* (Charles Scribner's Sons, New York, 1902).
  - [4] C. Shannon, Bell Syst. Tech. J. **27**, 379 (1948).
  - [5] L. Onsager, Annals of the New York Academy of Sciences **51**, 627 (1949).
  - [6] B. J. Alder and T. E. Wainwright, J. Chem. Phys. **27**, 1208 (1957).
  - [7] W. W. Wood and J. D. Jacobson, J. Chem. Phys. **27**, 1207 (1957).
  - [8] D. Frenkel, Physica A: Statistical Mechanics and its Applications **263**, 26 (1999).
  - [9] D. Frenkel, Nat. Mater. **14**, 9 (2015).
  - [10] U. Agarwal and F. A. Escobedo, Nat. Mater. **10**, 230 (2011).
  - [11] P. F. Damasceno, M. Engel, and S. C. Glotzer, Science **337**, 453 (2012), arXiv:1202.2177 [cond-mat.soft].
  - [12] A. P. Gantapara, J. de Graaf, R. van Roij, and M. Dijkstra, Phys. Rev. Lett. **111**, 015501 (2013).
  - [13] C. A. Mirkin, R. L. Letsinger, R. C. Mucic, and J. J. Storhoff, Nature **382**, 607 (1996).
  - [14] D. Nykypanchuk, M. M. Maye, D. van der Lelie, and O. Gang, Nature **451**, 549 (2008).
  - [15] S. Y. Park, A. K. R. Lytton-Jean, B. Lee, S. Weigand, G. C. Schatz, and C. A. Mirkin, Nature **451**, 553 (2008).
  - [16] M. M. Maye, M. T. Kumara, D. Nykypanchuk, W. B. Sherman, and O. Gang, Nat. Nano. **5**, 116 (2010).
  - [17] B. Srinivasan, T. Vo, Y. Zhang, O. Gang, S. Kumar, and V. Venkatasubramanian, Proc. Nat. Acad. Sci. U.S.A. **110**, 18431 (2013).
  - [18] A. Jain, J. R. Errington, and T. M. Truskett, Soft Matter **9**, 3866 (2013).
  - [19] A. Jain, J. R. Errington, and T. M. Truskett, Phys. Rev. X **4**, 031049 (2014).
  - [20] G. van Anders, D. Klotsa, N. K. Ahmed, M. Engel, and S. C. Glotzer, Proc. Natl. Acad. Sci. U.S.A. **111**, E4812 (2014), arXiv:1309.1187 [cond-mat.soft].
  - [21] G. van Anders, D. Klotsa, A. S. Karas, P. M. Dodd, and S. C. Glotzer, ACS Nano **9**, 9542 (2015), arXiv:1507.04960 [cond-mat.soft].
  - [22] S. C. Glotzer and M. J. Solomon, Nat. Mater. **6**, 557 (2007).
  - [23] Y. Xia, Y. Xiong, B. Lim, and S. Skrabalak, Angew. Chem., Int. Ed. **48**, 60 (2009).
  - [24] S. Sacanna and D. J. Pine, Curr. Opin. Colloid Interface Sci. **16**, 96 (2011).
  - [25] Z. Gong, T. Hueckel, G.-R. Yi, and S. Sacanna, Nature **550**, 234 (2017).
  - [26] D. Frenkel, J. Chem. Phys. **81**, 3188 (1984).
  - [27] G. van Anders, N. K. Ahmed, R. Smith, M. Engel, and S. C. Glotzer, ACS Nano **8**, 931 (2014), arXiv:1304.7545 [cond-mat.soft].

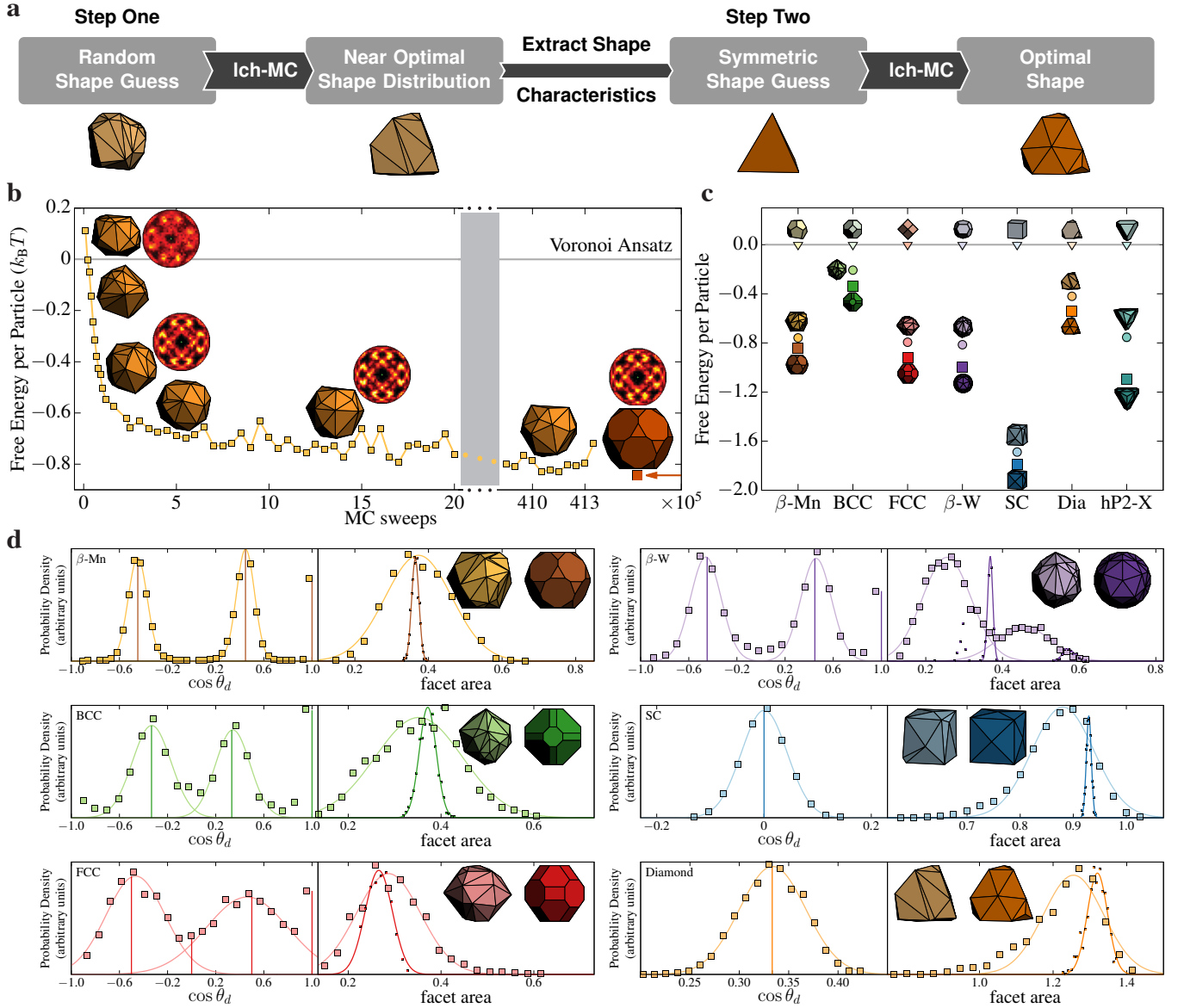


FIG. 1. **a** Schematic diagram illustrating the process. Alchemical Monte Carlo (Alch-MC) starts from a random convex shape and then finds an optimal shape for the  $\beta$ -Mn structure. PMFT isosurface of the optimal shape reveals that it has dodecahedral characteristics. In the second step, fluctuating particle shape alchemical Monte Carlo (Alch-MC) simulation starts from a dodecahedron and finds an optimal truncated dodecahedron for the  $\beta$ -Mn structure. **b** Alch-MC for the inverse design of a thermodynamically optimal hard particle shape to form a target (here,  $\beta$ -Mn) structure. The structure is imposed by an auxiliary design criterion, and detailed balance drives particles to take on shapes (selected shapes are displayed) that are favorable for the target structure (indicated by selected bond-order diagrams). Directly computed free energy confirms Alch-MC simulation over  $\gtrsim 10^5$  distinct shapes converges to shapes that have lower free energy (by  $\approx 0.8 k_B T$  per particle; numerical errors are smaller than markers) than shapes chosen by Voronoi construction. Desired shape features can be inferred from the equilibrium particle shape distribution and used to create a symmetry-restricted ansatz, which yields a thermodynamically optimal synthesizable shape. **c** Direct free energy comparison of precision engineering strategy for seven target structures:  $\beta$ -Mn, BCC, FCC,  $\beta$ -W, SC, diamond and hP2-X. For each structure we calculate the free energy of the target crystal for a shape formed from a geometric ansatz based on the Voronoi decomposition of the structure (triangles). Compared with the Voronoi ansatz, we find that alchemical Monte Carlo (Alch-MC) simulation over arbitrary convex polyhedra produces shapes (circles) that spontaneously self-assemble the target structures with lower free energy. Symmetry restricted polyhedra (squares) inferred from shapes in step one produce putatively thermodynamically optimal particle shapes by maximizing entropy. **d** Two-step shape alchemical Monte Carlo (Alch-MC) entropic particle-shape optimization for six target structures:  $\beta$ -Mn, BCC, FCC,  $\beta$ -W, SC and Diamond. For each target structure, an initial Alch-MC simulation over 92- or 188-dimensional spaces of convex polyhedra converged to highly faceted modifications of identifiable Platonic, Archimedean, or Catalan solids, obtained by calculation of the equilibrium distribution of the (left) cosine of dihedral angles ( $\cos \theta_d$ ) and (right) facet areas (Gaussian distributions are plotted with solid lines for comparison). In all cases, representative shapes spontaneously self-assembled target structures in  $NVT$  simulations. A second Alch-MC simulation over symmetry-restricted families of shapes determines a thermodynamically optimal shape. We show the mean of the cosine of dihedral angle distributions in SI Table S2.

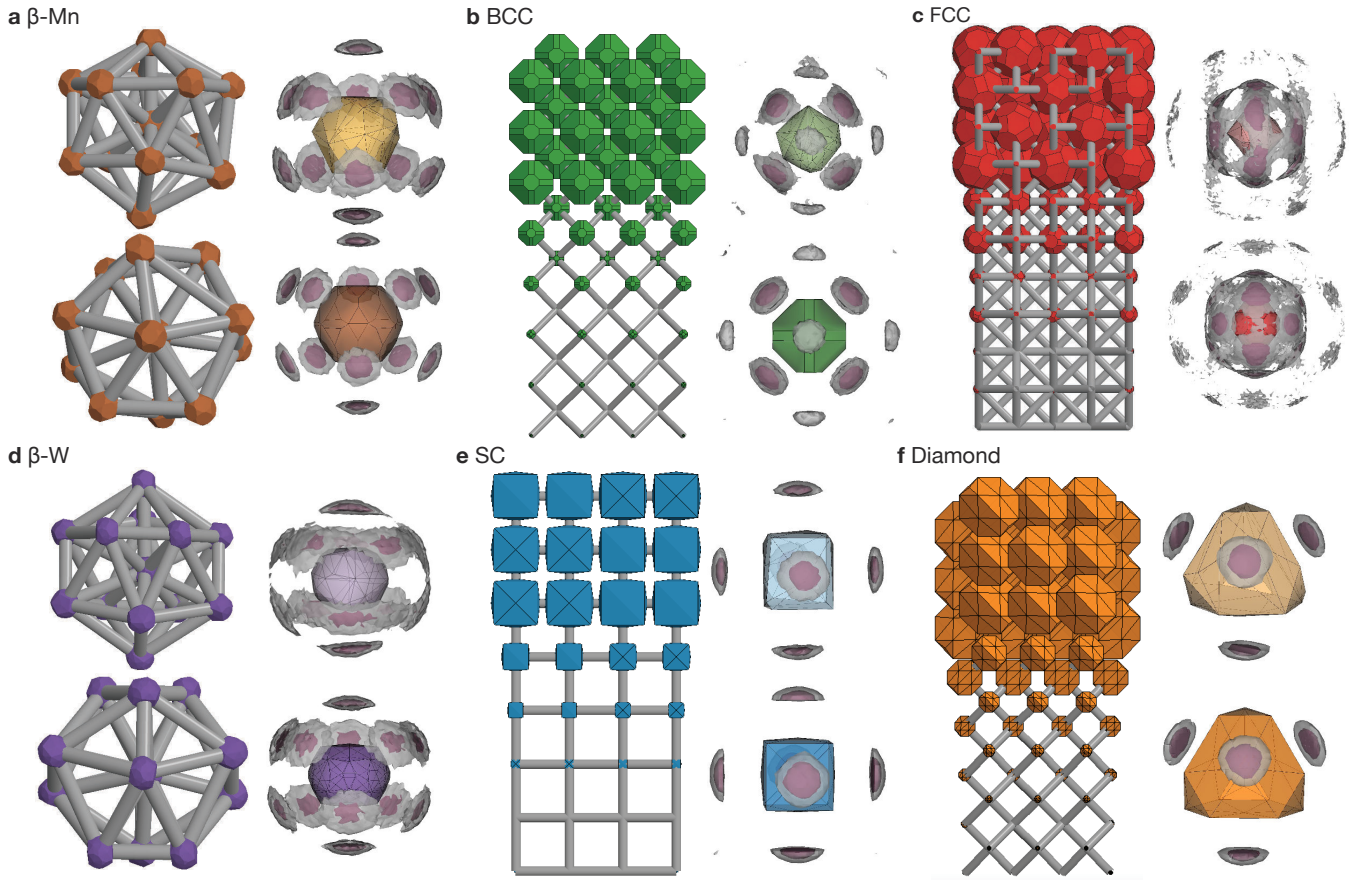


FIG. 2. Structure and potential of mean force and torque (PMFT) isosurfaces for optimal shapes in six target structures:  $\beta$ -Mn, BCC, FCC,  $\beta$ -W, SC and diamond. Each panel shows structural coordination (global: BCC, FCC, SC, diamond; local:  $\beta$ -Mn,  $\beta$ -W), and PMFT isosurfaces at free energy values of  $1.4 k_B T$  (light gray) and  $0.7 k_B T$  (pink) above the minimum value, for an optimal but unsymmetrized convex polyhedron (top) and for an optimal symmetry-restricted polyhedron (bottom). PMFT isosurfaces indicate emergence of particle faceting (see Fig. 2) corresponds with entropic valence localized at particle facets that preferentially align along crystal lattice directions. PMFT isosurfaces for symmetry-restricted polyhedra retain valence-lattice correspondence.



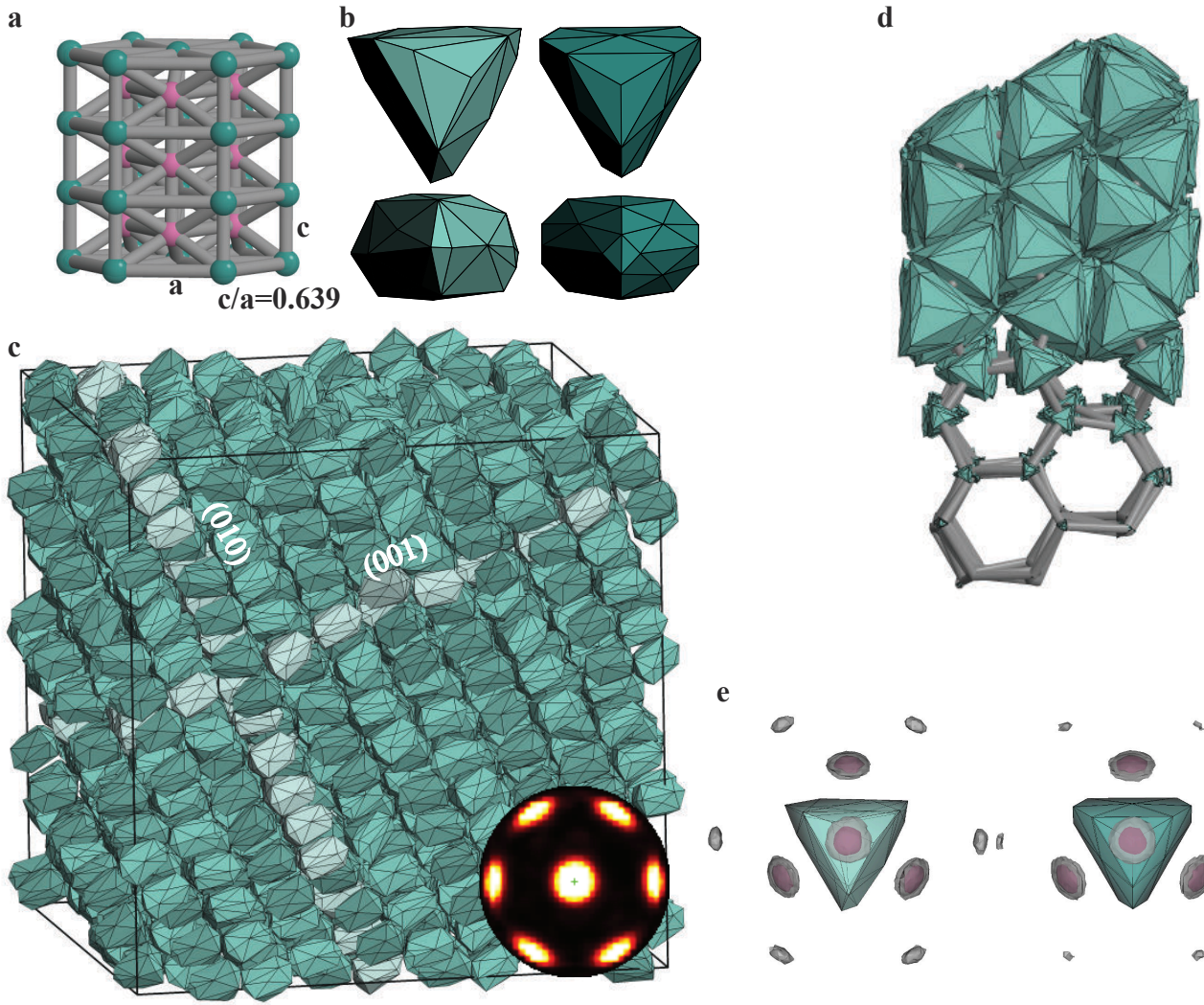


FIG. 3. Alch-MC design and self-assembly of a previously unreported novel crystal structure with no known atomic equivalent. **a** The structure is a distorted version of HCP with 8 rather than 12 nearest neighbors. Alch-MC simulation produces a particle (**b**) that spontaneously self-assembles the target structure (**c**) in simulation. Inset is a bond order diagram of the structure. **d** Particle organization relative to lattice directions. **e** PMFT isosurface for optimal shape.